

## Temperature-dependent phase separation within the Emery model

J. Carstensen and K. Dichtel

*Institut für Theoretische Physik der Universität Kiel, D-2300 Kiel, Germany*

(Received 9 March 1992; revised manuscript received 9 June 1992)

The variational principle of Bogoliubov, combined with a canonical transformation, is used to derive the thermodynamic functions for the hole-doped two-dimensional Emery model of the copper-oxygen planes in high-temperature-superconducting (HTSC) materials. A local ansatz and a transformation optimized for small values of the ratio of the hopping constant to the Coulomb correlation gives the lowest free energy in the neutral case and in the case of moderate doping. The regions of thermodynamic instability in the curves of the chemical potential versus doping, as coexistence regions of phase separation, are determined numerically with use of a Maxwell construction. In the high-doping regime, the coexistence regions are reduced considerably by the condition that the strong-coupling result is the lowest one, better than, e.g., the standard Hartree-Fock solution. The phase diagram of paramagnetic, ferromagnetic, antiferromagnetic, and separated phases is given. The parameter dependence of the maximum temperature of phase separation shows the same tendency as the empirical parameter dependence of the HTSC transition temperatures.

### I. INTRODUCTION

In the years immediately after the discovery of high-temperature superconductivity<sup>1</sup> (HTSC), both the still-unrevealed mechanism of this type of superconductivity and the unconventional properties of the normal electronic state have attracted much attention. In particular, in the low-doping regime of the hole-doped Cu oxide planes in HTSC materials, the Mott-Hubbard picture of strong electron correlation, instead of the standard band scheme, has been invoked to explain the isolating behavior, magnetic properties, and strange temperature dependence of transport properties which differ considerably from the usual Fermi-liquid behavior. (See Ref. 2 or 3, e.g., for a review for the latter.) The standard Hubbard model and its extension for the Cu-O planes, the Emery model,<sup>4</sup> taking into account the large on-site correlations on the Cu sites, still suffer from a lack of adequate calculational methods even for the equilibrium properties. Numerical solutions and variational Monte Carlo methods as applied by several groups<sup>5-10</sup> are—in spite of the tremendous numerical effort—of limited accuracy and in most cases restricted to a few lattice cells, low dimensions, small doping values, and temperatures not approaching zero. Thus expansions of the Hamiltonian for the infinite on-site correlation limit of the Hubbard models to the  $t$ - $J$  model<sup>11-13</sup> and analytical methods for this case of suppressed double occupancies such as the slave-boson method also are favored.<sup>14-17</sup> The advantage of this relatively simple mathematical treatment, however, is counterbalanced by the fact that the relation to small and intermediate values of correlation is completely lost in these methods; sometimes, even the validity of this standard strong-coupling limit is questioned.<sup>18-20</sup> So it seems worthwhile to apply a standard thermodynamic variational method, which has already been shown to be suitable for the strong-coupling regime of the neutral Hubbard model,<sup>21,22</sup> to the doped Emery model. The

most prominent features of the resulting temperature- and concentration-dependent phase diagrams in this paper are large regions of phase separation. Phase separation, as proposed by Vischer<sup>23</sup> for the non-neutral Hubbard model and suggested by Emery, Kivelson, and Lin<sup>24</sup> for the  $t$ - $J$  model, is assumed to result from competing tendencies of the carriers in correlated systems between the formation of antiferromagnetic bonds and of itinerant-carrier-concentration domains. Several recent papers confirm the occurrence of phase separation in correlated models, including ones which treat the one-dimensional  $t$ - $J$  model<sup>25-27</sup> and others which apply approximation methods to higher-dimensional models.<sup>7,14,15,28,29</sup> The occurrence of phase separation in small lattice-cluster calculations is still unclear as discussed in Refs. 8 and 30. The advantage of our variation calculation is the possibility to treat phase separation in the original Emery model with realistic parameter values. Of course, the nature of the nonhomogeneous solutions inside these coexistence regions still remains unknown and requires additional work. The existence of other inhomogeneous or incommensurate magnetic phases cannot be excluded, but the present calculations can serve to establish the parameter dependence of the region wherein unconventional electronic properties and probably HTSC occur.

### II. APPROXIMATION METHOD FOR THE GRAND CANONICAL POTENTIAL

We start with the Hamiltonian of the Emery model,<sup>4</sup>

$$\begin{aligned} \mathcal{H} &= U_d \mathcal{H}_{dd} - \varepsilon_0 \mathcal{N}_d + \gamma \mathcal{H}_1 \\ &= \frac{U_d}{2} \sum_{n,\sigma} x_{n,\sigma}^{1+} x_{n,\sigma}^1 x_{n,-\sigma}^{1+} x_{n,-\sigma}^1 - \varepsilon_0 \sum_{n,\sigma} x_{n,\sigma}^{1+} x_{n,\sigma}^1 \\ &\quad + \gamma \sum_{\langle n,(m,j) \rangle} (t_{n,(m,j)} x_{n,\sigma}^{1+} x_{m,\sigma}^j + \text{H.c.}) . \end{aligned} \quad (1)$$

The operator  $x_{n,\sigma}^{1+}$  creates  $3d$  holes on copper sites  $n$ , and the  $x_{n,\sigma}^{j+}$  operator creates  $2p_x$  for  $j=2$  and  $2p_y$  for  $j=3$  holes on nearest-neighbor  $\langle n,(m,j) \rangle$  oxygen sites. The transfer integral  $t_{n,(m,j)}$  takes the values  $\pm 1$  alternatively, corresponding to the symmetry between the Cu  $3d$  and O  $2p$  orbitals. In the following we set  $U_d=1$ , where  $U_d$  denotes the on-site repulsion between copper holes. The quantity  $\varepsilon_0$  denotes the charge-transfer energy between copper and oxygen holes. Extensions of our calculations to Hamiltonians including nearest-neighbor and oxygen correlations are possible.

We use the well-known variational principle of Bogoliubov in a form given in Ref. 31 and extended to the grand canonical potential in<sup>32</sup>

$$\Omega \leq \Omega_0(\mathcal{U}) = \Omega_T + \langle \mathcal{U}^\dagger \mathcal{H} \mathcal{U} \rangle_T - \langle \mathcal{H}_T + \mu \mathcal{N} \rangle_T \quad (2)$$

to get an upper bound for the grand canonical potential.  $\Omega_T$  is the grand canonical potential of the trial Hamiltonian, and  $\mathcal{N}$  denotes the total particle-number operator.  $\mathcal{U}$  is an arbitrary unitary transformation with  $[\mathcal{N}, \mathcal{U}] = 0$ , which allows for a larger variety of variational parameters without complicating the calculation of the traces in the expectation value  $\langle \cdots \rangle_T$ .

We choose the local trial Hamiltonian

$$\begin{aligned} \mathcal{H}_T = & \sum_{c_1, c_3} \frac{\tilde{u}_{c_1, c_3}}{2} \sum_{\sigma, n} x_{n,\sigma}^{c_1+} x_{n,\sigma}^{c_1} x_{n,-\sigma}^{c_3+} x_{n,-\sigma}^{c_3} \\ & + \sum_{n, c_1} h_n^{c_1} s_{z,n}^{c_1} - \tilde{\varepsilon}_0 \mathcal{N}_d - \lambda \mathcal{N}, \end{aligned} \quad (3)$$

with

$$s_{z,n}^{c_1} = \frac{1}{2} (x_{n,\uparrow}^{c_1+} x_{n,\uparrow}^{c_1} - x_{n,\downarrow}^{c_1+} x_{n,\downarrow}^{c_1}). \quad (4)$$

The variational parameters  $\tilde{u}_{c_1, c_3}$  describe effective correlations,  $\tilde{\varepsilon}_0$  an effective charge-transfer energy,  $\lambda$  some variational chemical potential (see Ref. 32 for the necessity

of its use), and  $h_n^{c_1}$  are antiferromagnetic (ferromagnetic) effective fields. As this Hamiltonian, the atomic limit in the lattice cell, separates in real space, all traces can be done analytically.

We choose the arbitrary transformation  $\mathcal{U}$  as to minimize  $\Omega_0$  to order  $\gamma^2$ :

$$\langle \mathcal{U}^\dagger \mathcal{H} \mathcal{U} \rangle_a = \langle \mathcal{H} \rangle_a + \gamma^2 M_s + o(\gamma^2), \quad (5)$$

where  $\langle \cdots \rangle_a$  denotes the expectation value with respect to the atomic limit ( $\gamma=0$ ). The procedure to find this optimal  $\mathcal{U}$  is strictly analogous to the one used in Ref. 21, but slightly more complicated because of the larger number of operators involved. In the special cases  $\varepsilon_0=0.5$  and 1, results are obtained which simplify the following transformations considerably:

$$\mathcal{U} = \exp[-2\varphi \exp(i\pi \mathcal{H}_{dd}) \mathcal{H}_2 \exp(-i\pi \mathcal{H}_{dd})] + o(\gamma^2) \quad (6)$$

$$= \exp \left[ -2\varphi \sum_{\substack{k, \sigma \\ i=1,2,3}} \varepsilon_k^i z_{k,\sigma}^i z_{k,\sigma}^i \right], \quad (7)$$

with

$$\mathcal{H}_2 = [\mathcal{N}_d, \mathcal{H}_1] \quad (8)$$

and

$$\varphi = \begin{cases} -\gamma, & \varepsilon_0 = \frac{1}{2} \\ -\frac{\gamma}{2}, & \varepsilon_0 = 1. \end{cases} \quad (9)$$

$$\varphi = \begin{cases} -\gamma, & \varepsilon_0 = \frac{1}{2} \\ -\frac{\gamma}{2}, & \varepsilon_0 = 1. \end{cases} \quad (10)$$

The three band energies and band operators  $\varepsilon_k^i$  and  $z_{k,\sigma}^i$  respectively, as is well known for the diagonalization of the hopping term of the Emery model, are defined in Appendix A, where the transformation from Eq. (6) to (7) is worked out explicitly.

For  $\varepsilon_0=0.5$  we obtain, with Eq. (5),

$$M_s = 2 \sum_{\langle n,(m,j) \rangle} \{ 2 \langle x_{n,-\sigma}^{1+} x_{n,-\sigma}^1 (x_{n,\sigma}^{1+} x_{n,\sigma}^1 - x_{m,\sigma}^{j+} x_{m,\sigma}^j) \rangle_a - \langle x_{n,\sigma}^{1+} x_{n,\sigma}^1 - x_{m,\sigma}^{j+} x_{m,\sigma}^j \rangle_a \}. \quad (11)$$

Because of  $\varepsilon_0 > 0$  and  $U_d \gg 0$ , the following inequalities hold for small doping values:

$$0 < \langle x_{n,\sigma}^{1+} x_{n,\sigma}^1 - x_{m,\sigma}^{j+} x_{m,\sigma}^j \rangle_a, \quad (12)$$

$$0 > \langle x_{n,-\sigma}^{1+} x_{n,-\sigma}^1 (x_{n,\sigma}^{1+} x_{n,\sigma}^1 - x_{m,\sigma}^{j+} x_{m,\sigma}^j) \rangle_a, \quad (13)$$

which prove that the transformation  $\mathcal{U}$  indeed lowers the grand canonical potential  $\Omega_0$  with respect to the atomic limit. In comparison to the Hubbard model, we see that in the Emery model dominant energy lowering is achieved from the last term, representing the different densities on copper and oxygen places.

In order to adapt our transformation to finite values of  $\gamma$  and to values  $\varepsilon_0 \neq 0.5$  or  $\varepsilon_0 \neq 1$ , we now take the ‘‘rotation angle’’  $\varphi$  in Eq. (7) as an additional variational parameter in  $\mathcal{U}$ . The operators  $z_{k,\sigma}^i$  then transform in a simple way:

$$\mathcal{U}^\dagger(\varphi) z_{k,\sigma}^i \mathcal{U}(\varphi) = \exp(-2\varphi \varepsilon_k^i) z_{k,\sigma}^i. \quad (14)$$

We perform the straightforward but lengthy calculation of the expectation value of the completely transformed Hamiltonian in Appendix B, where the functions  $u_{c_1, c_3}(\varphi)$ ,  $o_{c_1, c_3}(\varphi)$ , and  $q_{c_1, c_3}(\varphi)$  and the integrals  $G(0, c_1, \varphi)$  and  $F_1(0, c_1, \varphi)$  are defined, and get

$$\begin{aligned}
\langle \mathcal{U}^\dagger(\varphi) \mathcal{H} \mathcal{U}(\varphi) \rangle_T &= \sum_{c_1, c_3} u_{c_1, c_3}(\varphi) \frac{1}{2} \sum_{\sigma} (\langle x_{\sigma}^{c_1+} x_{\sigma}^{c_1} x_{-\sigma}^{c_3+} x_{-\sigma}^{c_3} \rangle_T - \frac{1}{N} \langle x_{\sigma}^{c_1+} x_{\sigma}^{c_1} \rangle_T \langle x_{-\sigma}^{c_3+} x_{-\sigma}^{c_3} \rangle_T) \\
&+ \sum_{c_1, c_3} o_{c_1, c_3}(\varphi) n^{c_1} n^{c_3} - \sum_{c_1, c_3} q_{c_1, c_3}(\varphi) s_z^{c_1} s_z^{c_3} \\
&+ 2\gamma \sum_{c_1, \sigma} \text{Re}[G(0, c_1, \varphi)] \langle x_{\sigma}^{c_1+} x_{\sigma}^{c_1} \rangle_T - \varepsilon_0 \sum_{c_1, \sigma} F_1(0, c_1, \varphi) \langle x_{\sigma}^{c_1+} x_{\sigma}^{c_1} \rangle_T.
\end{aligned} \tag{15}$$

The result for the grand canonical potential is

$$\begin{aligned}
\frac{\Omega_0}{N} &= \frac{\Omega_T}{N} + \frac{1}{N} \langle \mathcal{U}^\dagger(\varphi) \mathcal{H} \mathcal{U}(\varphi) \rangle_T - \sum_{c_1, c_3} \bar{u}_{c_1, c_3} \frac{1}{2} \sum_{\sigma} \langle x_{\sigma}^{c_1+} x_{\sigma}^{c_1} x_{-\sigma}^{c_3+} x_{-\sigma}^{c_3} \rangle_T \\
&- \sum_{c_1} h^{c_1} s_z^{c_1} + \bar{\varepsilon}_0 \sum_{\sigma} \langle x_{\sigma}^{1+} x_{\sigma}^1 \rangle_T + (\lambda - \mu) \sum_{c_1, \sigma} \langle x_{\sigma}^{c_1+} x_{\sigma}^{c_1} \rangle_T.
\end{aligned} \tag{16}$$

For the local expectation values of the hole densities and spin densities on the lattice sites  $n$ , we introduced the notations

$$n^c = \frac{1}{2} (\langle x_{\sigma}^{c+} x_{\sigma}^c \rangle_T + \langle x_{-\sigma}^{c+} x_{-\sigma}^c \rangle_T), \tag{17}$$

$$s_z^c = \frac{1}{2} (\langle x_{\sigma}^{c+} x_{\sigma}^c \rangle_T - \langle x_{-\sigma}^{c+} x_{-\sigma}^c \rangle_T), \tag{18}$$

where we dropped the lattice-site index  $n$  because of the translational invariance of  $\mathcal{H}_T$ . In the nonmagnetic case for  $h_n^{c_1} \equiv 0$ , all  $s_z^c$  vanish in the trial Hamiltonian (3). At low temperatures sometimes simple approximation formulas are used:

$$n^1 = \frac{n_h}{2} \quad \text{and} \quad n^2 = n^3 = 0 \quad \text{for } n_h < 1, \tag{19}$$

and

$$n^1 = \frac{1}{2} \quad \text{and} \quad n^2 = n^3 = \frac{n_h - 1}{4} \quad \text{for } n_h \geq 1, \tag{20}$$

with the total hole density, as given quantity for doped materials,

$$n_h = \frac{\langle \mathcal{U}^\dagger \mathcal{N} \mathcal{U} \rangle_T}{N} = \frac{\langle \mathcal{N} \rangle_T}{N} = 2(n^1 + n^2 + n^3). \tag{21}$$

### III. VARIATIONAL EQUATIONS

#### A. General formulation

Now we perform the complete minimization of the approximated grand canonical potential in Eq. (16) with respect to all variational parameters and obtain for  $\bar{u}_{c_1, c_3}$  the equation

$$\bar{u}_{c_1, c_3} = u_{c_1, c_3}(\varphi), \tag{22}$$

for  $\varepsilon_0$  and  $\lambda$

$$\begin{aligned}
0 &= \sum_{c_3} 2[-u_{c_1, c_3}(\varphi) + o_{c_1, c_3}(\varphi)] n^{c_3} \\
&+ 4\gamma \text{Re}[G(0, c_1, \varphi)] - 2\varepsilon_0 F(0, c_1, \varphi) + 2\bar{\varepsilon}_0 \delta_{c_1, 1} \\
&+ 2(\lambda - \mu) \quad (c_1 = 1, 2, 3)
\end{aligned} \tag{23}$$

and, for the antiferromagnetic fields  $h^{c_1}$ ,

$$0 = \sum_{c_3} 2[-u_{c_1, c_3}(\varphi) + q_{c_1, c_3}(\varphi)] s_z^{c_3} + h^{c_1} \quad (c_1 = 1, 2, 3). \tag{24}$$

In the ferromagnetic case, the last equation changes to

$$0 = \sum_{c_3} 2[-u_{c_1, c_3}(\varphi) + o_{c_1, c_3}(\varphi)] s_z^{c_3} + h^{c_1} \quad (c_1 = 1, 2, 3). \tag{25}$$

The evaluation of the grand canonical potential  $\Omega_0$  has to be done with the minimal parameter values from these equations and with the optimized  $\varphi$ .

#### B. Expansions for small values of $\varphi$

In the following we always get a first insight into the variational equations by some expansion in  $\varphi$  for approximately half filling before presenting numerical results. As mentioned above, the leading and numerically dominating terms in Eq. (15) are not the correlation terms, but the expressions linear in density or better density differences between copper and oxygen sites:

$$\sum_{\sigma} \{ \langle x_{\sigma}^{1+} x_{\sigma}^1 \rangle_T - \langle x_{\sigma}^{j+} x_{\sigma}^j \rangle_T \}.$$

Thus, minimizing the prefactor of this sum to order  $\varphi^2$ ,

$$h(\varphi) = 2\varepsilon_0 \varphi^2 + 2\gamma \varphi, \tag{26}$$

which means

$$\varphi = -\frac{\gamma}{2\varepsilon_0} \tag{27}$$

yields the first approximation, which shows that small values of the charge-transfer energy  $\varepsilon_0$  produce the same tendencies in the model as large values of the transfer integral  $\gamma$ . As a first example, we discuss Eq. (23) for the level renormalization approximatively to order  $\gamma^2$ :

$$(\bar{\varepsilon}_0 - \varepsilon_0) = \gamma^2 \left\{ \left[ \frac{4}{\varepsilon_0} - \frac{1}{\varepsilon_0^2} \right] (n^2 + n^3 - n^1) + \frac{6}{\varepsilon_0} \right\}, \tag{28}$$

which shows that for  $\varepsilon_0 > 0.25$  the value of variational charge transfer is enhanced for all doping values.

An approximation of the optimal  $\varphi$  to order  $\varphi^4$  from Eq. (15) can be given in the same way. With

$$a = \frac{\gamma}{\varepsilon_0}, \quad (29)$$

we get

$$\varphi \approx \frac{a^3}{3(a^2 + \frac{1}{10})} - \frac{a}{2}. \quad (30)$$

For the values, e.g.,  $\gamma = 0.1$  and  $\varepsilon_0 = 0.5$ , we have

$$\varphi = -0.081, \quad (31)$$

which means an error of less than 1% of the numerical value.

We use this expansion to give approximate values of the effective correlations:

$$u_{1,1} = 1 - 32\Phi_2 + \frac{1312}{3}\Phi_4 + o(\varphi^4), \quad (32)$$

$$u_{1,2} = 4\Phi_2 - \frac{272}{3}\Phi_4 + o(\varphi^4), \quad (33)$$

$$u_{2,2} = 32\Phi_4 + o(\varphi^4), \quad (34)$$

$$u_{2,3} = 16\Phi_4 + o(\varphi^4), \quad (35)$$

with

$$\Phi_2 = \varphi^2 + 2\gamma\varphi \quad \text{and} \quad \Phi_4 = \varphi^4 + 4\gamma\varphi^3. \quad (36)$$

Retaining only the leading second-order terms with  $\Phi_2 = -\gamma^2$  for  $\varepsilon_0 = 0.5$ , e.g., we find an enhancement of the on-site copper correlation  $u_{1,1}$  and an effective attractive copper-oxygen correlation  $u_{1,2} = -\gamma^2$ . But we should remember as well as for the result  $\tilde{\varepsilon}_0 - \varepsilon_0$  above that these values are only variational parameters to adjust optimally the spectrum of the trial Hamiltonian to the real spectrum in the energy region of the most important contributions to the thermodynamic quantities.

## IV. RESULTS

### A. Variational free energy

We pass in the usual way from the grand canonical potential  $\Omega_0$  to the free energy as the thermodynamic quantity for fixed hole concentration  $n_h$ :

$$F_0(n_h, T) = \Omega_0(\mu(n_h, T)) + n_h \mu(n_h, T). \quad (37)$$

In the following our results are compared with the standard paramagnetic Hartree-Fock (HF) mean-field (MF) results for the Emery model as established, e.g., in Refs. 33 and 34 and obtained within our method with a generalized one-particle trial Hamiltonian. Figures 1 and 2 show the free energy (our method, HF, and atomic limit) as a function of the doping concentration  $n_h$  for some strong-coupling case  $\gamma = 0.05$  and for some intermediate value  $\gamma = 0.1$ , respectively. One sees that the qualitative behavior, especially the discontinuities in slope at the neutral concentration value  $n_h = 1$  of our curves, resembles those in the atomic limit, as expected from our an-

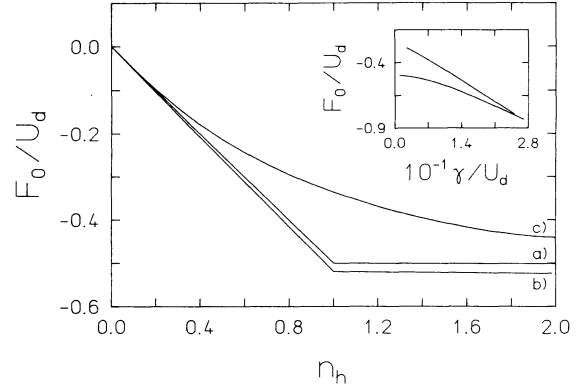


FIG. 1. Free energy  $F_0/U_d$  vs hole concentration  $n_h$  for  $\gamma/U_d = 0.05$  and  $\varepsilon_0/U_d = 0.5$ . Atomic limit (curve a), strong-coupling variational method (curve b), and Hartree-Fock solution as weak-coupling limit (curve c). Inset, free energy vs  $\gamma/U_d$  for  $n_h = 1$ . Upper curve, Hartree-Fock; lower curve, strong-coupling method.

satz, whereas the (paramagnetic) HF solution passes smoothly the neutral concentration. On this energy scale, with considerable energy differences between the weak- and strong-coupling free-energy solutions, the much smaller energy differences between solutions of different magnetic symmetry are nearly invisible; thus, we restrict ourselves to the paramagnetic HF solution for comparison. As the insets for the neutral case in both figures show, the difference between the HF and our solution increases with decreasing  $\gamma$  and increasing  $\varepsilon_0$ , as already indicated in the optimal  $\varphi$  in Eq. (26). We also observe in the latter curve a smooth dependence on  $\varepsilon_0$ , proving the suitability of our solution in the complete interval  $\varepsilon_0 > 0$  despite the fact that, as described above, our transformation was optimized only for  $\varepsilon_0 = 0.5$  and 1. Of course, the free-energy difference to the atomic limit increases for larger values of the hopping constant  $\gamma$ .

Equation (11) shows that our strong-coupling solution gives the best free energy for half filling, where the difference

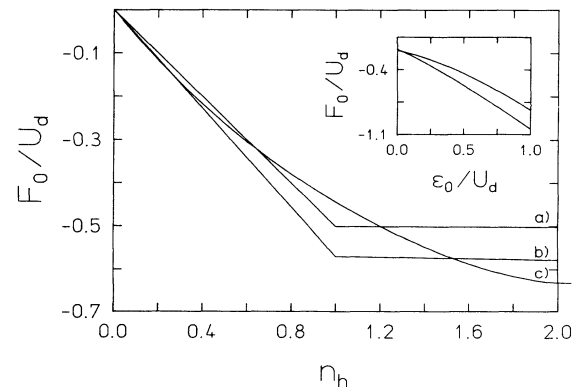


FIG. 2. Same as Fig. 1 for  $\gamma/U_d = 0.1$ . Inset, free energy vs charge-transfer energy  $\varepsilon_0/U_d$  for  $n_h = 1$ . Upper curve, Hartree-Fock; lower curve, strong-coupling method.

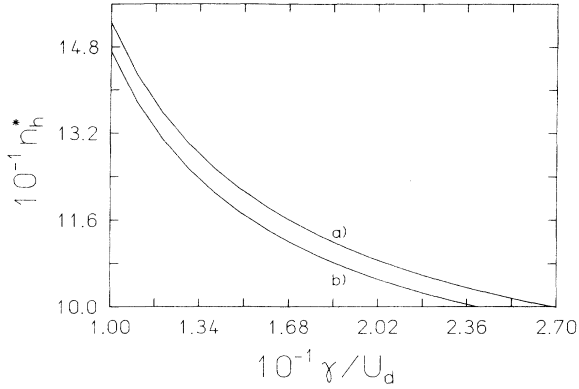


FIG. 3. Critical concentration  $n_h^*$  as a function of  $\gamma/U_d$  (a) for  $\epsilon_0/U_d=0.5$  and (b) for  $\epsilon_0/U_d=0.4$ . Only in the region below this curve does phase separation occur.

$$\langle x_{n,\sigma}^{1+} x_{n,\sigma}^1 - x_{m,\sigma}^{j+} x_{m,\sigma}^j \rangle_T \quad (38)$$

has its maximum. Thus our strong-coupling solution dominates in the small (hole and electron) doping regime, whereas for larger values of  $n_h$  the HF curve is lower. This fact is consistent with the common observation that the standard band structure and mean-field picture fail in the low-doping nonmetallic region of HTSC materials. The (temperature dependent) critical doping concentration  $n_h^*$  as the separation line between both solution types is shown in Fig. 3 as a function of the hopping constant  $\gamma$  for two values of  $\epsilon_0$ . Only for values of  $\gamma$  less some  $\gamma_{\max}(\epsilon_0)$  does an interval of positive carrier concentration exist, where our method improves the HF solution and phase separation, as described below, occurs.

The HF solution is only used as a first indication of the limits of the validity of our solution; better solutions could further reduce  $n_h^*$ . Comparison with the numerical results of other authors is difficult, despite the large number of existing materials on this topic, because most calculations in the literature are done on the one-band Hubbard or  $t$ - $J$  model. Only few calculations for the (finite  $U_d$ ) Emery model are available such as in Ref. 10. In Fig. 4 we took the Gutzwiller energy of Fig. 1 in Ref. 10

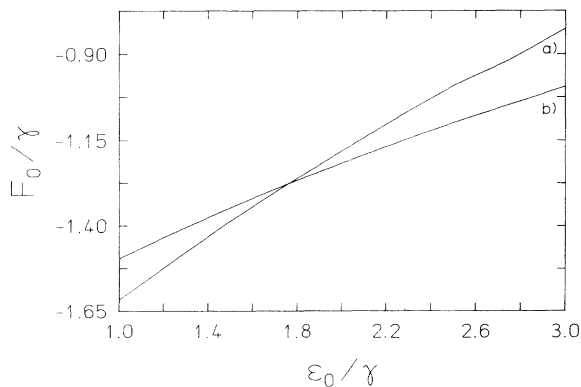


FIG. 4. Free energy vs charge transfer  $\epsilon_0/U_d$  for comparison: (a) result of Fig. 1 in Ref. 10; (b) our results for same on site correlation  $U_d/\gamma=8$  and same energy scale.

and plotted our low-temperature free energy for the same energy scale and parameter values versus  $\epsilon_0$ . For small values of  $\epsilon_0$ , the former one is better, whereas with increasing charge-transfer values our (upper bound) gives lower energies, according to the fact that increasing  $\epsilon_0$  reduces the effective hopping and favors our solution.

## B. Magnetic order

We now proceed from the paramagnetic case described above to magnetic phases with  $h_n^{c_1} \neq 0$  in the trial Hamiltonian (3) and the MF equations (24) and (25). Within this paper we restrict our trial Hamiltonian to collinear magnetic phases; generalizations to spiral phases, however, are possible. As discussed in Ref. 21, expectation values of physical quantities are to be calculated from the operators transformed with  $\mathcal{U}$  because we chose a transformed Hamiltonian as the trial Hamiltonian. First, we consider the spin-dependent site occupancies and obtain, with the methods of Appendix B for the antiferromagnetic case,

$$\langle \mathcal{U}^\dagger x_{n,\sigma}^{j+} x_{n,\sigma}^j \mathcal{U} \rangle_T = \sum_{c_1} F_j(0, c_1, \varphi) n^{c_1} \pm F_j(Q, j, \varphi) s_z^j \quad (39)$$

and, for the ferromagnetic case,

$$\langle \mathcal{U}^\dagger x_{n,\sigma}^{j+} x_{n,\sigma}^j \mathcal{U} \rangle_T = \sum_{c_1} F_j(0, c_1, \varphi) (n^{c_1} \pm s_z^j), \quad (40)$$

where the upper (lower) sign holds for spin up (down). As in Eq. (16), these expectation values contain the temperature-dependent quantities  $n^{c_1}$  and  $s_z^{c_1}$ , which have to be determined from  $\Omega_T$  now with  $h_n^{c_1} \neq 0$ . With the approximations of Eq. (20) and correspondingly  $s_z^{c_1} = 0$  for  $c_1 = 2, 3$  for half filling, we see that only the copper sites ( $j=1$ ) contribute to the second (antiferromagnetic) term in Eq. (39), as expected for antiferromagnetic order in these materials.

For extreme low temperatures ( $\beta h^1 \gg 1$ ), we have

$$s_z^1 \equiv \frac{1}{2} \text{sgn}(h^1). \quad (41)$$

As established from numerical calculations, the magnetic phase transitions are of second order only near to  $n_h = 1$  and then the only relevant quantity is  $h_1$ . For antiferromagnetic (AF) order and low temperature, the molecular-field equation then becomes, with Eq. (24),

$$h^1 = (u_{1,1} - q_{1,1}) 2s_z^1 \approx -32\Phi_4 \text{sgn}(h_1) \approx 0.00542. \quad (42)$$

(The numerical value is for  $\epsilon_0 = 0.5$  and in units of  $[U_d]$  confirmed by the complete numerical evaluations.) In the same way the ferromagnetic equation becomes, with Eq. (25) and approximation to order  $\varphi^4$ ,

$$h^1 = (u_{1,1} - o_{1,1}) 2s_z^1 = (o_{1,1} - u_{1,1}) \text{sgn}(h_1) = o(\varphi^4), \quad (43)$$

which shows that to order  $\gamma^4$  there is no ferromagnetism

for  $n_h = 1$ .

For small values of  $h^1$  ( $\beta h^1 \ll 1$ ) near to the magnetic phase transition, we linearize in  $h^1$ . Near half filling we obtain, with Eq. (20),

$$s_z^1 = -\beta \frac{h^1}{4} \quad (44)$$

and, for the antiferromagnetic case,

$$h^1 = (u_{1,1} - q_{1,1}) 2s_z^1 \approx -32\Phi_4 \beta \frac{h^1}{2} \quad (45)$$

or

$$k_B T_N = -16\Phi_4. \quad (46)$$

Taking, e.g.,  $\varepsilon_0 = 0.5$  and  $\varphi = -\gamma$  gives the approximation for the Néel temperature:

$$k_B T_N = 48\gamma^4. \quad (47)$$

Antiferromagnetism appears as a phenomenon in order  $\gamma^4$ , as expected in superexchange theory. Considering Eq. (47) as a MF approximation of the Heisenberg AF model, an exchange constant  $J_{\text{eff}} = 48\gamma^4$  results, which agrees with the standard strong-coupling expansion of the Emery model given in, e.g., Ref. 19. Taking in Eq. (46) as the better approximation for  $\varphi$  of Eq. (30) for  $\varepsilon_0 = 0.5$  and  $\gamma = 0.1$ , we find

$$\frac{T_N}{U_d} = 29 \text{ K/eV}, \quad (48)$$

which is, for  $U_d = 10$  eV, in very good agreement with our numerical results and the experimental value for  $\text{La}_2\text{CuO}_4$ .

The free-energy differences for different magnetic phases are not visible in the scale of Figs. 1 and 2. [The phase diagram Fig. 7 shows that antiferromagnetism (without phase separation) is indeed restricted to hole concentrations less 1.01.] Ferromagnetism occurs in the phase diagram only for large hole concentrations, as expected.

### C. Phase separation

The most interesting fact from the numerical results is the occurrence of phase separation. The curve  $\mu$  versus  $n_h$  in Fig. 5 shows not only the charge-transfer gap at  $n_h = 1$  (overestimated in this local approximation scheme compared with Monte Carlo results and spectroscopic experiments), but also large regions of instability, i.e., of negative slope  $\partial\mu/\partial n_h < 0$ . The inset in Fig. 5 is an enlarged picture of the nearly constant part of the upper curve. As is well known, this instability region corresponds to some concave part in the free energy  $F_0$ . Replacing this part by a common tangent produces the standard Maxwell construction (see, e.g., Ref. 35 or in an application to the one-band Hubbard model<sup>16</sup>). The constant values of  $\mu$  and free energies above are evaluated using this construction. Tracing back to the origin of the negative slope  $n_h$  versus  $\mu$ , we consider Eq. (23), which connects  $\mu$  and the variational parameter  $\lambda$  in our expansion to order  $\varphi^4$ ,

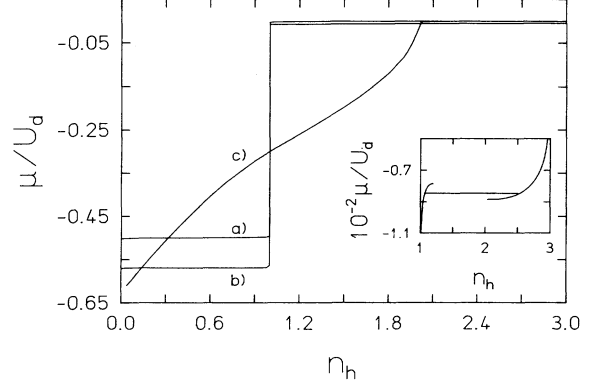


FIG. 5. Chemical potential  $\mu/U_d$  versus  $n_h$  for  $\varepsilon_0/U_d = 0.5$  and  $\gamma/U_d = 0.1$  shows the “charge transfer” discontinuity at  $n_h = 1.0$ . Atomic limit (curve *a*), strong-coupling variational method (curve *b*), and Hartree-Fock solution as weak-coupling limit (curve *c*). Inset, enlarged part of the constant line for  $n_h > 1$ . Both branches can only be connected by a part of negative slope of  $\mu$ . A Maxwell construction in the free energy determines  $\mu$  in the coexistence region.

$$(\lambda - \mu) \approx \left\{ -4\Phi_2 + \frac{272}{3}\Phi_4 \right\} n^1 - 40\Phi_4(n^2 + n^3) + 8\gamma\left(\varphi - \frac{40}{3}\varphi^3\right) + 8\varepsilon_0\left(\varphi^2 - \frac{20}{3}\varphi^4\right), \quad (49)$$

with the abbreviations  $\Phi_2$  and  $\Phi_4$  defined in Eq. (36). Inserting our first approximation to the optimal  $\varphi$  of Eq. (27) and differentiation with respect to  $n_h$  leads to

$$\left[ \frac{\partial\lambda}{\partial n_h} - \frac{\partial\mu}{\partial n_h} \right] \approx \gamma^2 \left[ \frac{4}{\varepsilon_0} - \frac{1}{\varepsilon_0^2} \right] \frac{\partial n^1}{\partial n_h} + \gamma^4 \left[ \frac{8}{\varepsilon_0^3} - \frac{1}{\varepsilon_0^4} \right] \left[ -\frac{17}{3} \frac{\partial n^1}{\partial n_h} + \frac{5}{2} \frac{\partial(n^2 + n^3)}{\partial n_h} \right]. \quad (50)$$

As our trial Hamiltonian  $\mathcal{H}_T$  describes a system of  $\delta$ -like densities of states, passing a spike causes large variations in  $n_h$  for only small variations in  $\lambda$ . Then the extremely small values of the derivative  $\partial\lambda/\partial n_h$  can (as the right-hand side is positive in our parameter range) only be compensated by some negative  $\partial\mu/\partial n_h$ . Note that phase separation occurs within this approximation as a consequence of narrow bands in the highly correlated limit, quite independent of the magnetic-field equations (24) and (25). Thus we expect the phenomenon to persist even in calculations including more magnetic phases of different symmetry. For small temperatures near half filling, we again use the approximation (19) for the expectation values with the trial Hamiltonian and see that phase separation is a phenomenon of second order determined by the quantity  $\Phi_2$  for  $n_h < 1$  and of fourth order in  $\gamma$  determined by the quantity  $\Phi_4$  for  $n_h > 1$ . Differentiating to  $\varepsilon_0$  at fixed  $\gamma$ , we obtain  $\varepsilon_{0 \text{ optimal}} = 0.5$  for  $n_h < 1$  and  $\varepsilon_{0 \text{ optimal}} = \frac{1}{6}$  for  $n_h > 1$ . Then it follows that the lower the

temperature, the larger  $\gamma$ , and in our parameter range the lower  $\epsilon_0$ , the more is the tendency of carriers to separate into regions of low concentration  $n_1$  and high concentration  $n_2$ . For a specimen with given  $n_h$ , there are three possibilities.

- (i)  $n_h < n_1$ : One nearly neutral phase exists.
- (ii)  $n_1 \leq n_h \leq n_2$ : Two phases exist whose concentrations  $n_1$  and  $n_2$  for some given temperature  $T$  are determined from the intersection of the line  $T = \text{const}$  with the curves in the phase diagrams Fig. 6 or 7, respectively.
- (iii)  $n_h > n_2$ : Only one phase of high concentration exists.

Figure 6 shows the temperature-dependent coexistence regions of phase separation between paramagnetic phases. We see that phase separation does not occur only between phases of different magnetic order as suggested by Refs. 23 and 24, but seems to be a phenomenon inherent to this type of strong-coupling solution. The coexistence regions evaluated numerically for three values of  $\gamma$  are reduced drastically by the ‘‘Hartree-Fock limiting curve,’’ which means, as shown in Fig. 2, that, for concentrations larger than  $n_h^*$ , the Hartree-Fock solution with one homogeneous phase becomes the better one. The parts of the coexistence curves on the right-hand side of the figure then only serve to determine at a given  $T$  and  $n_h$  the carrier concentration  $n_2$  of the domains with high concentration (note that  $n_2 \gg n_h$  is possible).

The reduced coexistence regions (hatched regions in Figs. 6 and 7) show a strong parameter dependence. If one expects interesting phenomena such as superconductivity within these regions, a subtle optimization problem arises: For  $\gamma$  too large,  $n_h^*$  becomes too small, and the Hartree-Fock line bounding the coexistence region from the right approaches the coordinate axis of neutral concentration. If, on the contrary,  $\gamma$  is too small, the maximum temperatures reached become too small. The same

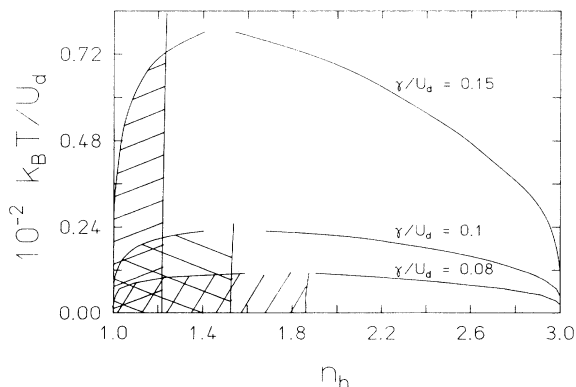


FIG. 6. Phase diagram of the carrier-separated paramagnetic states for  $\epsilon_0/U_d = 0.5$  and different values of  $\gamma/U_d$ . The (hatched) coexistence region in the phase diagram is bounded to the right by the ‘‘Hartree-Fock limiting curve’’ at  $n_h^*$ . A large coexistence region—perhaps enclosing the region of unconventional electronic properties and HTSC—is a matching process: for  $\gamma/U_d$  too large,  $n_h^*$  becomes too small; for  $\gamma/U_d$  too small, only small maximum temperatures are reached.

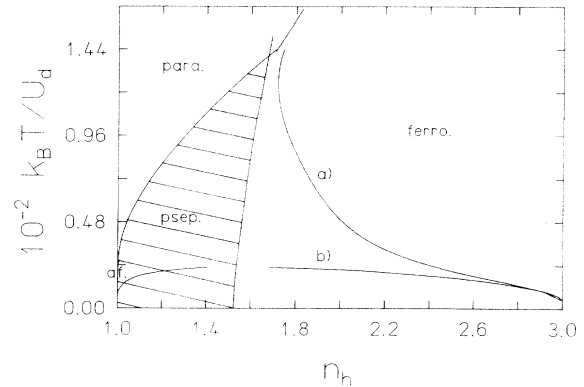


FIG. 7. Phase diagram for  $\epsilon_0/U_d = 0.5$  and  $\gamma/U_d = 0.1$  (a) of separated states between antiferromagnetic (paramagnetic for high temperatures) and ferromagnetic states [the (hatched) coexistence region is again reduced by the ‘‘Hartree-Fock limiting curve’’] and (b) for comparison only as in Fig. 6 between paramagnetic states.

matching problem holds for  $1/\epsilon_0$ .

Figure 7 shows the complete phase diagram including magnetic order, where the coexistence region is rather enlarged. A phase-transition line between paramagnetism and ferromagnetism meets the top of the phase-separating region at some critical point. Again, the HF limiting curve reduces the coexistence region considerably and makes this critical region irrelevant for this parameter set. If one assumes these phase-separated regions to be a necessary condition for HTSC (regions of high doping eventually join in some percolative manner<sup>36</sup>), then the abrupt change to the HF solution at  $n_h^*$  would give an explanation to the puzzling breakdown of HTSC at still rising carrier concentration  $n_h$ , which is otherwise difficult to understand.

Despite the fact that in the case of phase separation a theory of inhomogeneous superconductivity would be required, we compare our maximum attainable temperature of phase separation  $T_{\text{max}}$  with the empirical parameter dependence of  $T_c$  in Ref. 37. Figure 3(a) in Ref. 37 shows that  $T_c$  increases with decreasing  $\Delta V_M$  and Fig. 9 there shows that  $T_c$  increases with increasing  $t$ . If we identify the charge-transfer constant  $\Delta V_M \approx \epsilon_0$  and, according to Ref. 38,  $t = \gamma^2/\epsilon_0$ , our results show roughly the same parameter dependence for  $T_{\text{max}}$ . These parameter tendencies are consistent with the fact that the critical concentration  $n_h^*$  is in a region where considerable changes in symmetry and experimental quantities (for the sign of the Hall coefficient, e.g., see Ref. 3) take place, a hint that phase separation may be fundamental in HTSC.

## V. CONCLUSIONS

A strong-coupling solution scheme with carrier phase separation dominates the low-doping regime of copper-oxygen planes until some critical doping, where the mean-field Hartree-Fock solution starts to give lower variational free energies. For lower (higher) tempera-

tures, the system separates between antiferromagnetic (paramagnetic) nearly neutral regions and regions of high carrier concentration up to some maximum temperature. Calculations on correlated models in the non-neutral case should take into account this subtle phenomenon possibly revealed by the numerical error in Monte Carlo calculations.

### ACKNOWLEDGMENTS

The authors are highly indebted to Professor H. Koppe, Kiel, for his continuing interest in this work and for many suggestions, to Professor K. A. Müller, Zürich, for an encouraging discussion, and to Professor R. J. Jelitto, Frankfurt, for making available to us his work on the Hubbard model as well as those of his collaborators.

### APPENDIX A: UNITARY TRANSFORMATION

We define new operators

$$a_{n,\sigma}^j = \exp(i\pi\mathcal{H}_{dd})x_{n,\sigma}^j \exp(-i\pi\mathcal{H}_{dd}) \quad (\text{A1})$$

or, explicitly,

$$a_{n,\sigma}^1 = x_{n,\sigma}^1 (1 - 2x_{n,-\sigma}^1 x_{n,-\sigma}^1), \quad (\text{A2})$$

$$a_{n,\sigma}^j = x_{n,\sigma}^j, \quad j=2,3. \quad (\text{A3})$$

Since

$$a_{n,\sigma}^{1+} a_{n,\sigma}^1 = x_{n,\sigma}^{1+} x_{n,\sigma}^1, \quad (\text{A4})$$

holds, this transformation is inverted by

$$x_{n,\sigma}^1 = a_{n,\sigma}^1 (1 - 2a_{n,-\sigma}^1 a_{n,-\sigma}^1). \quad (\text{A5})$$

Introducing the standard Fourier-transformed operators

$$a_{k,\sigma}^j = N^{-1/2} \sum_n \exp[-ik(R_n + R^j)] a_{n,\sigma}^j, \quad (\text{A6})$$

we can write

$$\exp(i\pi\mathcal{H}_{dd})\mathcal{H}_2 \exp(-i\pi\mathcal{H}_{dd})$$

$$= \sum_{\langle n,(m,j) \rangle} (t_{n,(m,j)} a_{n,\sigma}^{1+} a_{m,\sigma}^j - \text{H.c.}) \quad (\text{A7})$$

$$= \sum_{k,\sigma} \sum_j (\pm i s_j a_{k,\sigma}^{1+} a_{k,\sigma}^j - \text{H.c.}), \quad (\text{A8})$$

with

$$s_j \equiv 2 \sin \left[ \frac{k_j}{2} \right] \quad (j=2,3), \quad (\text{A9})$$

the plus sign holds for  $j=2$  and the minus sign holds for  $j=3$ .

Defining

$$B(k) = [s_2^2(k) + s_3^2(k)]^{1/2}, \quad (\text{A10})$$

Eq. (A8) is diagonalized with eigenvalues  $\varepsilon_k^j$  and eigenvectors  $z_{k,\sigma}^{j+}$  in the following way:

$$\varepsilon_k^1 = -iB(k), \quad (\text{A11})$$

$$z_{k,\sigma}^{1+} = \frac{1}{\sqrt{2}B(k)} [-B(k)a_{k,\sigma}^{1+} + s_2 a_{k,\sigma}^{2+} - s_3 a_{k,\sigma}^{3+}], \quad (\text{A12})$$

$$\varepsilon_k^2 = 0, \quad (\text{A13})$$

$$z_{k,\sigma}^{2+} = \frac{1}{B(k)} (s_3 a_{k,\sigma}^{2+} + s_2 a_{k,\sigma}^{3+}), \quad (\text{A14})$$

$$\varepsilon_k^3 = iB(k), \quad (\text{A15})$$

$$z_{k,\sigma}^{3+} = \frac{1}{\sqrt{2}B(k)} [B(k)a_{k,\sigma}^{1+} + s_2 a_{k,\sigma}^{2+} - s_3 a_{k,\sigma}^{3+}], \quad (\text{A16})$$

Now we can write

$$\exp(i\pi\mathcal{H}_{dd})\mathcal{H}_2 \exp(-i\pi\mathcal{H}_{dd}) = \sum_{\substack{k,\sigma \\ i=1,2,3}} \varepsilon_k^i z_{k,\sigma}^{i+} z_{k,\sigma}^i, \quad (\text{A17})$$

which shows that Eq. (7) holds. To write the eigenvectors in a short form, we define the unitary transformation  $T_k$ :

$$a_{k,\sigma}^{i+} = \sum_j T_k^{ji} z_{k,\sigma}^{j+}. \quad (\text{A18})$$

### APPENDIX B: EXPECTATION VALUES

The expectation value of the transformed operator  $\langle \mathcal{U}^\dagger \mathcal{H}_{dd} \mathcal{U} \rangle_T$  is calculated by expressing  $\mathcal{H}_{dd}$  in terms of  $z_{k,\sigma}^b$ , applying Eq. (14), and after all expressing  $\mathcal{H}_{dd}$  in terms of  $x_{n,\sigma}^i$  again. Defining

$$f_i(k,c,\varphi) = \sum_b T_k^{ib} \exp(2\varphi \varepsilon_k^b) T_k^{cb*}, \quad (\text{B1})$$

$$g_2(k,c,\varphi) = +i s_2(k) f_2(k,c,\varphi), \quad (\text{B2})$$

$$g_3(k,c,\varphi) = -i s_3(k) f_3(k,c,\varphi), \quad (\text{B3})$$

$$g(k,c,\varphi) = g_2(k,c,\varphi) + g_3(k,c,\varphi), \quad (\text{B4})$$

$$F_i(q,c,\varphi) = \frac{1}{N} \sum_k f_i(k,c,\varphi) f_i(k-q,c,-\varphi), \quad (\text{B5})$$

$$G(q,c,\varphi) = \frac{1}{N} \sum_k f_1(k,c,\varphi) g(k-q,c,-\varphi), \quad (\text{B6})$$

we get

$$\begin{aligned}
\langle \mathcal{U}^\dagger \mathcal{H}_{dd} \mathcal{U} \rangle_T &= \frac{1}{N^3} \sum_{\substack{k_1, k_2, k_3, k_4, \\ c_1, c_2, c_3, c_4, \\ n_1, n_2, n_3, n_4}} \left\{ \delta(-k_1 + k_2 - k_3 + k_4) f_1(k_1, c_1, \varphi) f_1(k_2, c_2, -\varphi) \right. \\
&\quad \times f_1(k_3, c_3, \varphi) f_1(k_4, c_4, -\varphi) \exp\{ik_1(R_{n_1} + R^{c_1}) - ik_2(R_{n_2} + R^{c_2})\} \\
&\quad \times \exp\{ik_3(R_{n_3} + R^{c_3}) - ik_4(R_{n_4} + R^{c_4})\} \\
&\quad \left. \times \frac{1}{2} \sum_{\sigma} \langle x_{n_1, \sigma}^{c_1+} x_{n_2, \sigma}^{c_2} x_{n_3, \sigma}^{c_3+} x_{n_4, -\sigma}^{c_4} \rangle_T \right\}. \tag{B7}
\end{aligned}$$

Antiferromagnetism is introduced here in the standard way by a set of molecular fields  $h_n^j$  ( $j=1,2,3$ ) alternating from lattice cell to lattice cell. Defining the vector

$$Q = (\pi, \pi), \tag{B8}$$

Eq. (B7) can be written (equivalent to Ref. 22) in the form

$$\begin{aligned}
\frac{\langle \mathcal{U}^\dagger \mathcal{H}_{dd} \mathcal{U} \rangle_T}{N} &= \sum_{c_1, c_3} \left\{ \frac{1}{N} \sum_q \{F_1(q, c_1, \varphi) F_1(q, c_3, \varphi) \exp[iq(R^{c_1} - R^{c_3})]\} \right. \\
&\quad \times \frac{1}{2} \sum_{\sigma} \{ \langle x_{\sigma}^{c_1+} x_{\sigma}^{c_1} x_{-\sigma}^{c_3+} x_{-\sigma}^{c_3} \rangle_T - \langle x_{\sigma}^{c_1+} x_{\sigma}^{c_1} \rangle_T \langle x_{-\sigma}^{c_3+} x_{-\sigma}^{c_3} \rangle_T \} \\
&\quad + \sum_{c_1, c_3} F_1(0, c_1, \varphi) F_1(0, c_3, \varphi) n^{c_1} n^{c_3} \\
&\quad \left. - \sum_{c_1, c_3} F_1(Q, c_1, \varphi) F_1(Q, c_3, \varphi) \exp[iQ(R^{c_1} - R^{c_3})] s_2^{c_1} s_2^{c_3} \right\}. \tag{B9}
\end{aligned}$$

In an equivalent way, we get

$$\frac{\langle \mathcal{U}^\dagger \mathcal{N}_d \mathcal{U} \rangle_T}{N} = \sum_{c_1, \sigma} \{F_1(0, c_1, \varphi) \langle x_{\sigma}^{c_1+} x_{\sigma}^{c_1} \rangle_T\} \tag{B10}$$

and

$$\mathcal{H}_1 = \sum_{\langle n, (m, j) \rangle_{\sigma}} t_{n, (m, j)} x_{n, \sigma}^{1+} x_{m, \sigma}^j + \text{H.c.} \tag{B11}$$

$$= \sum_{\langle n, (m, j) \rangle_{\sigma}} t_{n, (m, j)} (1 - 2a_{n, -\sigma}^{1+} a_{n, -\sigma}^1) a_{n, \sigma}^{1+} a_{m, \sigma}^j + \text{H.c.}, \tag{B12}$$

leading to

$$\begin{aligned}
\frac{\langle \mathcal{U}^\dagger \mathcal{H}_1 \mathcal{U} \rangle_T}{N} &= \sum_{c_1, \sigma} \{G(0, c_1, \varphi) \langle x_{\sigma}^{c_1+} x_{\sigma}^{c_1} \rangle_T\} + \text{H.c.} \\
&\quad - 4 \sum_{c_1, c_3} \left\{ \frac{1}{N} \sum_q \{F_1(q, c_1, \varphi) G_1(q, c_3, \varphi) \exp[iq(R^{c_1} - R^{c_3})]\} \right. \\
&\quad \times \frac{1}{2} \sum_{\sigma} \{ \langle x_{\sigma}^{c_1+} x_{\sigma}^{c_1} x_{-\sigma}^{c_3+} x_{-\sigma}^{c_3} \rangle_T - \langle x_{\sigma}^{c_1+} x_{\sigma}^{c_1} \rangle_T \langle x_{-\sigma}^{c_3+} x_{-\sigma}^{c_3} \rangle_T \} \left. \right\} + \text{H.c.} \\
&\quad - 4 \sum_{c_1, c_3} \{F_1(0, c_1, \varphi) G_1(0, c_3, \varphi) n^{c_1} n^{c_3}\} + \text{H.c.} \\
&\quad + 4 \sum_{c_1, c_3} \{F_1(Q, c_1, \varphi) G_1(Q, c_3, \varphi) \exp[iQ(R^{c_1} - R^{c_3})] s_2^{c_1} s_2^{c_3}\} + \text{H.c.} \tag{B13}
\end{aligned}$$

We define a function  $\bar{u}_{c_1, c_3}(\varphi)$  summing up all coefficients in  $\langle \mathcal{U}^\dagger \mathcal{H}_1 \mathcal{U} \rangle_T / N$  of the term

$$\langle x_{\sigma}^{c_1+} x_{\sigma}^{c_1} x_{-\sigma}^{c_3+} x_{-\sigma}^{c_3} \rangle_T - \langle x_{\sigma}^{c_1+} x_{\sigma}^{c_1} \rangle_T \langle x_{-\sigma}^{c_3+} x_{-\sigma}^{c_3} \rangle_T$$

and get a symmetric function

$$u_{c_1, c_3} = \frac{\bar{u}_{c_1, c_3} + \bar{u}_{c_3, c_1}}{2}. \quad (\text{B14})$$

In an equivalent way, we define the symmetric function  $q_{c_1, c_3}(\varphi)$  summing up all coefficients of  $s_z^{c_1} s_z^{c_3}$  and the function  $o_{c_1, c_3}(\varphi)$  by summing up all coefficients of  $n^{c_1} n^{c_3}$ . With these definitions, we get Eq. (15).

- 
- <sup>1</sup>J. G. Bednorz and K. A. Müller, *Z. Phys. B* **64**, 189 (1986).  
<sup>2</sup>K. Levin, J. H. Kim, J. P. Lu, and Q. Si, *Physica C* **175**, 449 (1991).  
<sup>3</sup>N. P. Ongin, *Physical Properties of High Temperature Superconductors*, Vol. II, edited by D. M. Ginsberg (World Scientific, Singapore, 1990).  
<sup>4</sup>V. J. Emery, *Phys. Rev. Lett.* **58**, 2794 (1987).  
<sup>5</sup>R. T. Scalettar, *Physica C* **162-164**, 313 (1989).  
<sup>6</sup>G. Dopf, A. Muramatsu, and W. Hanke, *Phys. Rev. B* **41**, 9264 (1990).  
<sup>7</sup>N. E. Bonesteel and J. W. Wilkins, *Phys. Rev. Lett.* **66**, 1232 (1991).  
<sup>8</sup>E. Dagotto, A. Moreo, F. Ortolani, J. Riera, and D. J. Scalapino, *Phys. Rev. Lett.* **67**, 1918 (1991).  
<sup>9</sup>S. R. White, D. J. Scalapino, R. L. Sugar, E. Y. Loh, J. E. Gubernatis, and R. T. Scalettar, *Phys. Rev. B* **40**, 506 (1989).  
<sup>10</sup>S. N. Coppersmith, *Phys. Rev. B* **41**, 8711 (1990).  
<sup>11</sup>V. A. Kapustin, *Fiz. Tverd. Tela (Leningrad)* **16**, 804 (1974) [*Sov. Phys. State* **16**, 520 (1974)].  
<sup>12</sup>K. A. Chao, J. Spalek, and A. M. Oleś, *J. Phys. C* **10**, L271 (1977).  
<sup>13</sup>J. Zaanen and A. M. Oleś, *Phys. Rev. B* **37**, 9423 (1988).  
<sup>14</sup>M. Grilli, R. Raimondi, C. Castellani, C. Di Castro, and G. Kotliar, *Phys. Rev. Lett.* **67**, 259 (1991).  
<sup>15</sup>G. Castellani, M. Grilli, and G. Kotliar, *Phys. Rev. B* **43**, 8000 (1991).  
<sup>16</sup>E. Arrigoni and G. C. Strinati, *Phys. Rev. B* **44**, 7455 (1991).  
<sup>17</sup>J. Brinckmann and N. Grewe, *Z. Phys. B* **84**, 179 (1991).  
<sup>18</sup>B. Friedman, X. Y. Chen, and W. P. Su, *Phys. Rev. B* **40**, 4431 (1989).  
<sup>19</sup>V. J. Emery and G. Reiter, *Phys. Rev. B* **38**, 4547 (1988).  
<sup>20</sup>F. C. Zhang and T. M. Rice, *Phys. Rev. B* **41**, 7243 (1990).  
<sup>21</sup>M. Heise and R. J. Jelitto, *Z. Phys. B* **25**, 381 (1976).  
<sup>22</sup>M. Heise and R. J. Jelitto, *Z. Phys. B* **26**, 177 (1977).  
<sup>23</sup>P. B. Vischer, *Phys. Rev. B* **10**, 943 (1974).  
<sup>24</sup>V. J. Emery, S. A. Kivelson, and H. Q. Lin, *Phys. Rev. Lett.* **64**, 475 (1990).  
<sup>25</sup>F. F. Assaad and D. Würtz, *Phys. Rev. B* **44**, 2681 (1991).  
<sup>26</sup>C. S. Hellberg and E. J. Mele, *Phys. Rev. Lett.* **67**, 2080 (1991).  
<sup>27</sup>M. Ogata, M. U. Luchini, S. Sorella, and F. F. Assaad, *Phys. Rev. Lett.* **66**, 2388 (1991).  
<sup>28</sup>A. Auerbach and B. E. Larson, *Phys. Rev. B* **43**, 7800 (1991).  
<sup>29</sup>M. Marder, N. Papanicolaou, and G. C. Psaltakis, in *Dynamics of Magnetic Fluctuations in HTSC*, edited by G. Reiter *et al.* (Plenum, New York, 1991).  
<sup>30</sup>H. Fehske, V. Waas, H. Röder, and H. Büttner, *Phys. Rev. B* **44**, 8473 (1991).  
<sup>31</sup>H. Koppe, in *Werner Heisenberg und die Physik unserer Zeit*, edited by F. Bopp (Vieweg, Braunschweig, 1961).  
<sup>32</sup>A. Huber, in *Boulder Lectures in Theoretical Physics*, edited by K. T. Mahanthappa and W. E. Brittin (Gordon and Breach, New York, 1969), Vol. XI D, p. 355.  
<sup>33</sup>X. Y. Chen, W. P. Su, C. S. Ting, and D. Y. Xing, *Solid State Commun.* **67**, 349 (1988).  
<sup>34</sup>S. N. Coppersmith and P. B. Littlewood, *Phys. Rev. B* **42**, 3966 (1990).  
<sup>35</sup>K. Huang, *Statistical Mechanics* (Wiley, New York, 1963).  
<sup>36</sup>V. Hizhnyakov, N. Kristoffel, and E. Sigmund, *Physica C* **161**, 435 (1988).  
<sup>37</sup>Y. Ohta, T. Tohyama, and S. Maekawa, *Phys. Rev. B* **43**, 2968 (1991).  
<sup>38</sup>F. C. Zhang and T. M. Rice, *Phys. Rev. B* **37**, 3759 (1988).